DAΦNE TECHNICAL NOTE

INFN - LNF, Accelerator Division

Frascati, August 29, 1995

Note: **MM-9**

MEASUREMENTS AND TUNING OF DAΦNE ACCUMULATOR DIPOLES

A, Battisti, B. Bolli, F. Iungo, F. Losciale, M. Paris,
M. Preger, C. Sanelli, F. Sardone, F. Sgamma, M. Troiani, S. Vescovi

1. Introduction

The DAΦNE Accumulator is a 32.56 m machine, used as a damping and accumulation ring for electrons and, alternatively, positrons designed to make injection into the collider main rings easier and faster [1]. The lattice of the Accumulator consists of four quasi-achromatic arcs, each one with two 45° bending magnets. In order to reduce the damping times as much as possible, a rather large operating field (1.55T) has been chosen, together with a vertically focusing gradient to achieve the optimum field index (n=0.5) for the damping distribution and a smooth behaviour of the betatron functions in the arcs.

Being the Accumulator essentially a steady state machine, a solid H-shaped yoke has been designed. The drawing in Figure 1 shows the main dimensions of the magnet, realized by TESLA Engineering [2] as a subcontractor of Oxford Instruments [3]. Figure 2 is a picture of the magnet mounted on a rotatable support to allow full magnetic mapping. Table I lists the main parameter of the bending magnet, as proposed by TESLA Engineering after checking the original design proposed by LNF.

TABLE I - Parameters of the DAΦNE Accumulator bending magnet

	Nominal		Maximum
Bending field (T)	1.545		1.66
Field index		0.5	
Gradient (T/m)	0.703		0.755
Bending radius (m)		1.1	
Deflection angle (deg)		45	
Magnetic Length (mm)		864.0 ± 0.8	
Pole gap at centre (mm)		42.00 ± 0.05	
Good field region (mm)		±30	
Field quality (ΔB/B)		$\leq 7.5 \times 10^{-4}$	
Ampere Turns/pole (A)	28080		30600
Turns per pole		48	
Current (A)	585		637.5
Conductor size (mm)		12x12	
Coolant hole diameter (mm)		7	
Current density (A/mm^2)	5.55		6.05
Magnet resistance (mΩ)		41	
Magnet Power (kW)	13.9		16.5
Number of water circuits		6	
Total flow rate (liters/minute)	10.0		11.8
Total pressure drop (Bar)	0.4		0.5
Temperature rise (°C)		20	

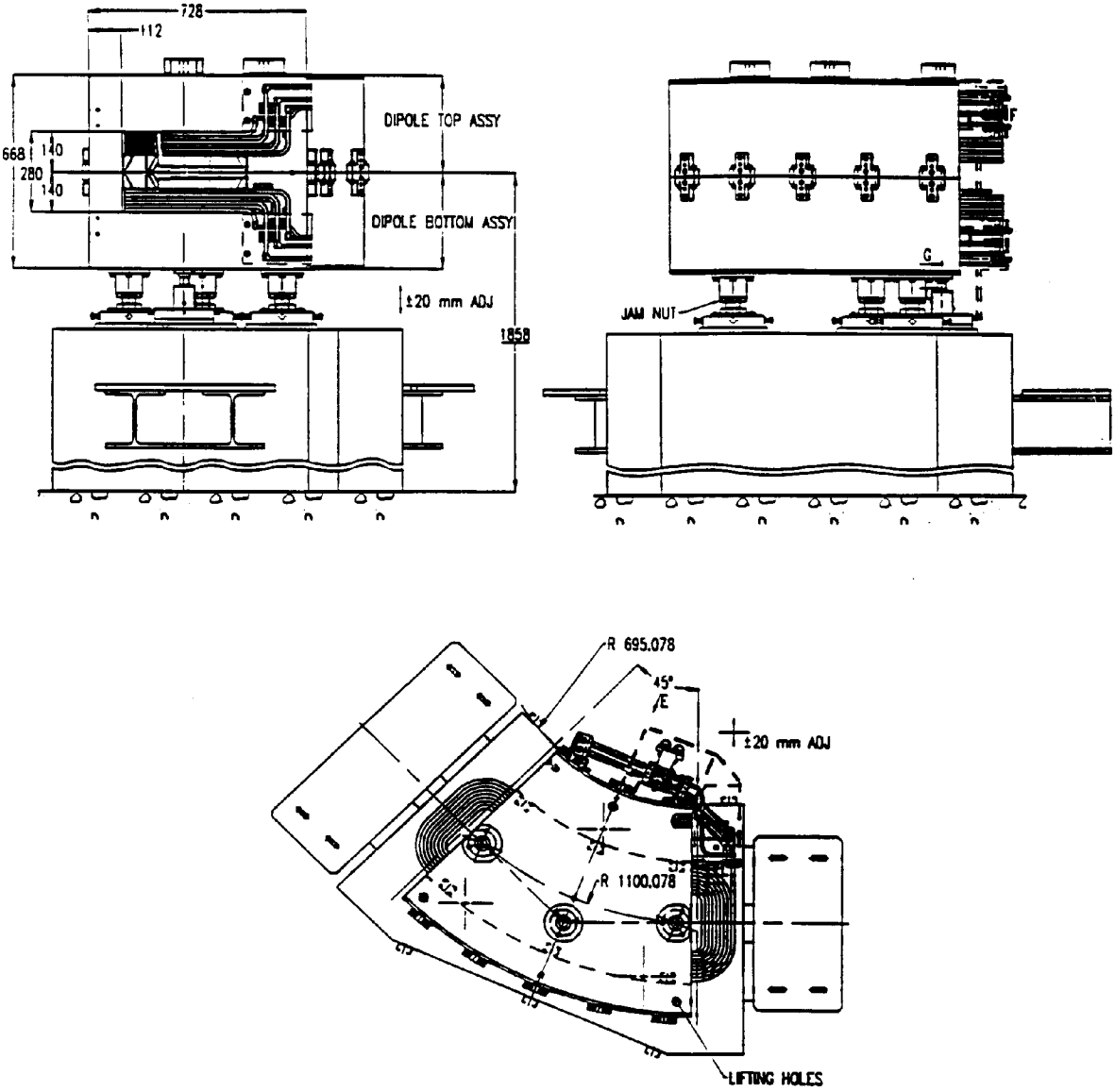

Figure 1 - Main sizes of the Accumulator dipole.

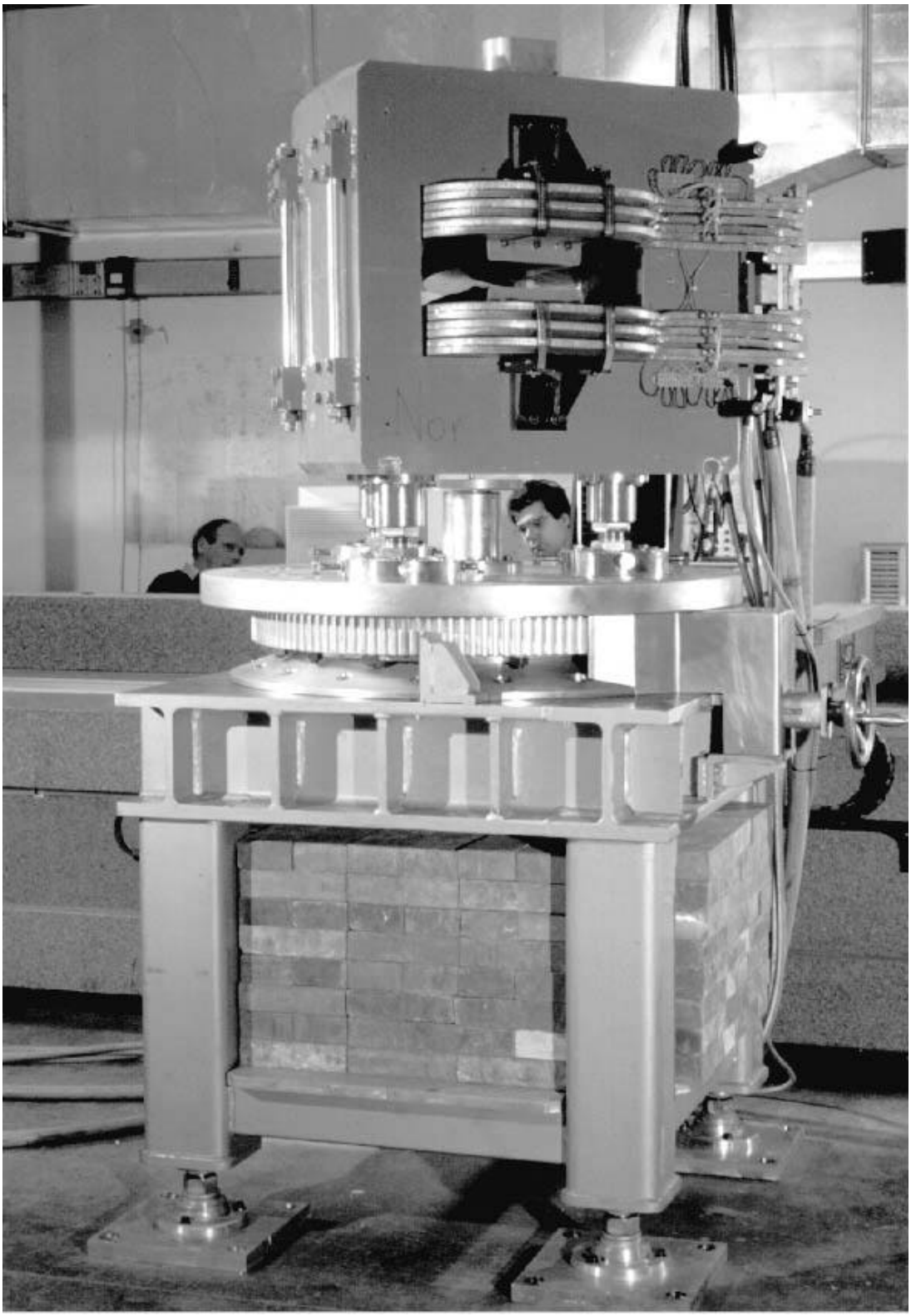

Figure 2 - The Accumulator dipole prototype on its rotating support for magnetic measurements.

2. Electrical measurements

The dipole prototype has been completely characterized at Tesla before shipment according to the Specification. The resistance of the entire magnet, measured at 23°C ambient temperature, was 39 mΩ.

The resistance measurement has been repeated at Frascati a first time using an OM20 microohmmeter and a second time by the Volt-Ampere method. Both measurements have been performed at 23 °C. We got the following results:

OM20:	39	mΩ
Volt-Ampere method	39.2	mΩ

The Volt-Ampere measurement has been performed at 591.05 A, measured by means of a precise DCCT, reading a voltage of 23.16 V at the bus-bars lugs.

The inductance of the magnet, and its frequency dependence, was measured by means of the L-R-C meter HP 4284A. The following table lists the results:

TABLE II - Inductance and resistance as a function of frequency

f (Hz)	R (Ω)	L (mH)
20	0.742	8.381
100	1.945	4.707
1000	7.573	2.054
10000	27.324	1.141

3. Hydraulic and thermal measurements

The nominal water flow rate has been measured at Tesla showing a good agreement with the basic parameter list (Table I). The measured values were:

ΔP = 0.4 bar Water Flow = 12.2 L/min

Thermal measurements have been performed at Frascati. The results are listed in the following.

TABLE III - Thermal measurements on the dipole prototype coils

H_2O Input Temp. °C	H_2O Output Upper Coil °C	H_2O Output Lower Coil °C	Copper Upper Coil °C	Time minutes
16.5	16.5	16.5	16.5	0
16.5	25.5	27.0	21.0	5
16.5	26.0	27.5	21.0	10
17.0	26.0	27.5	21.2	15
17.2	26.0	27.5	21.5	20
17.2	26.2	28.0	21.5	25
17.5	26.5	28.0	21.7	30
17.5	26.5	28.0	21.7	35

4. Magnetic measurements on the first prototype

The original pole profile, designed by LNF and accepted by TESLA, is shown in Figure 3, while Table IV gives the coordinates of the points shown in the figure. It is a shimmed profile, which leaves a field deviation from the ideal linear behavior, which is almost antisymmetric with respect to the magnet centre. As explained in the following, this profile failed in reaching the desired field quality and has been changed to a flat one, the results being described in the next section. To make comparison easier, both profiles are shown in the Figure and in the Table.

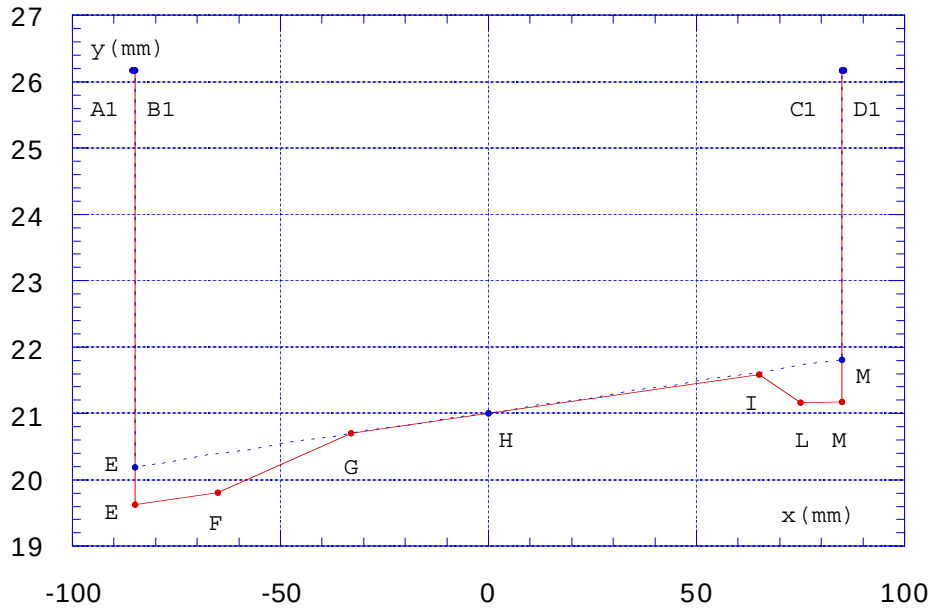

Figure 3 - Original shimmed (full line) and flat (dotted line) pole profiles.

TABLE IV - Coordinates of original and modified flat profiles

	x(mm)	y_{old} (mm)	y_{new}(mm)
A1	-85.43	26.170	26.170
B1	-85.00	26.170	26.170
E	-85.00	19.630	20.189
F	-65.00	19.810	
G	-33.00	20.700	
H	0.00	21.000	21.000
I	65.00	21.590	
L	75.00	21.160	
M	85.00	21.170	21.863
C1	85.00	26.170	26.170
D1	85.42	26.170	26.170

The prototype has been delivered for the first time to LNF in August 1994. After aligning the magnet with respect to the measurement bench, a Hall probe (GROUP3 MPT-141) has been positioned at the magnet center and the field measured as a function of the excitation current. The result is shown in Figure 4. The behaviour is linear below ≈400 A, while the nominal working point (1.545 T, corresponding to ≈595 A) is well within the saturation region.

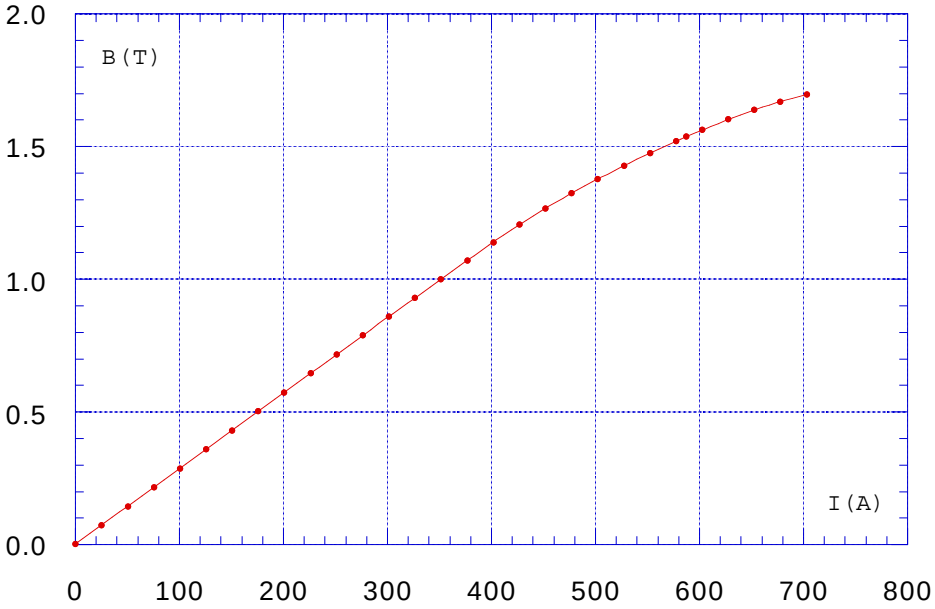

Figure 4 - Excitation curve.

We then measured the field at the magnet center in the direction perpendicular to the nominal trajectory to check the field quality within the required good field region. The measured field is shown in Figure 5. The horizontal coordinate has been chosen as positive towards the outside of the ring, where the gap is larger (see Figure 3), with the origin at the magnet centre. The good field region is within the two vertical full lines.

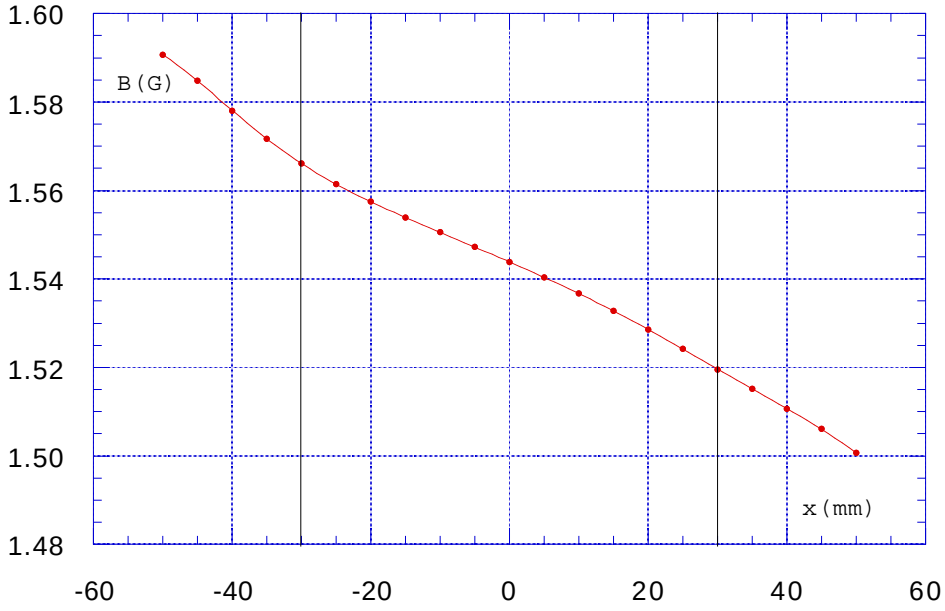

Figure 5 - Vertical field at magnet centre as a function of horizontal position.

In order to give a correct estimate of the field quality at the magnet centre within the specified good field region, we have established the following procedure:

- Measure the field along a straight line perpendicular to the nominal trajectory at the magnet centre.

- Calculate the gradient, defined as the first order coefficient of a linear fit to the measured points restricted to a small number of points around the magnet centre.

- Define the fractional deviation from the ideal field as the difference between the measured points and the corresponding ones on the linear fit, divided by the values of the linear fit.

This definition of the field quality was not clearly stated at the time of designing the magnet. In fact, applying the above defined criterion to the calculated field at the magnet centre, we find a gradient of 0.656 T/m, corresponding to n = 0.465, and the field quality is ≈±0.1%.

After applying this procedure to the measured points plotted in Figure 5, we found a gradient of 0.675 T/m, corresponding to a field index n = 0.481. Figure 6 shows the fractional deviation of the points in Figure 5 from the ideal linear field with this gradient. The full line in the figure shows, for comparison, the predictions of the 2-dimensional code POISSON used to design the magnet. The discrepancy is larger than the specified field quality. A comparison has been made also with the actual pole profile, mechanically measured by TESLA, which was anyway within the mechanical tolerance, but the discrepancy did not change significantly. The measured field quality at the good field region boundary is ≈±0.2%, more than twice the specified value.

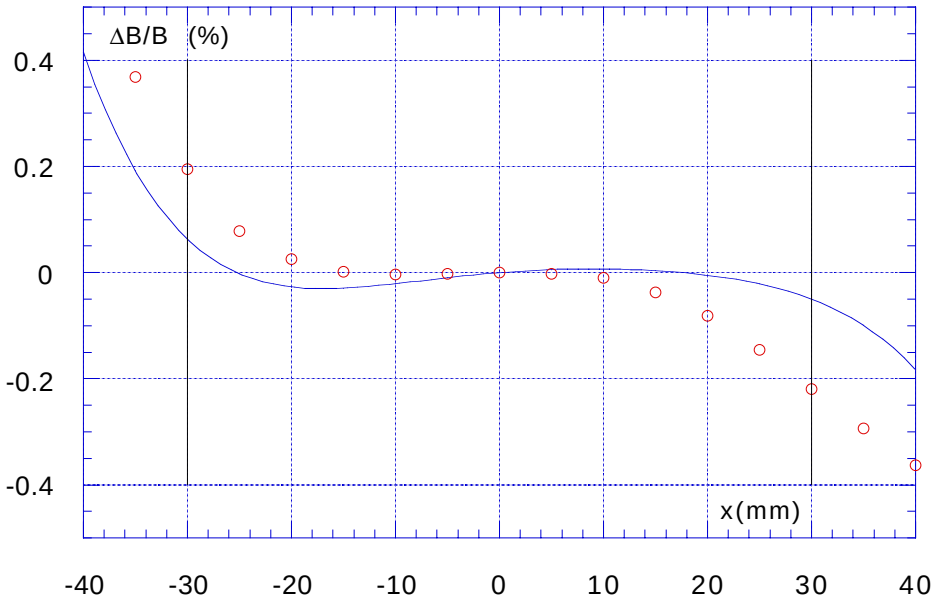

Figure 6 - Fractional deviation of the measured points from the linear field with G = 0.675 T/m (dots). The full line shows the calculated field.

Non linear contributions to the fringing field have been estimated by performing scans of the field along straight lines perpendicular to the nominal trajectory at several positions along it, concentrated around the end caps. Tracking tests including these estimates and the results described above near the magnet centre indicated a strong reduction in the storage ring acceptance. For this reason we decided to change the pole shape to a flat one, with the main justification of changing the high order component contributions from octupole-type to sextupole, which can be more easily handled by changing the settings of the lumped sextupoles in the lattice.

POISSON runs with the flat pole profile indicated in Figure 3 and Table IV indicated that a field quality very near to the specified one could be obtained.

The magnet has been therefore sent back to TESLA for the pole modification. The prototype has been delivered again to LNF in January 1995.

5. Measurements on the final prototype

Before the delivery of the magnet a rotating support has been realized, which allows to perform a complete mapping of the field (see Figure 2).

To get a longitudinal map along (or parallel to) the ideal trajectory, we start the measurement by positioning the Hall probe ≈35 cm outside the yoke to measure the behaviour of the fringing field, and then proceed inward until we reach the magnet centre. Then the Hall probe is extracted from the gap, the dipole rotated by 135° and the other half magnet measured as well.

The dipole is aligned in such a way that its mechanical centre (tooling hole) coincides with the rotation axis of the support. The two angular positions of the rotating support, corresponding to the two above defined positions of the magnet, are then fixed by setting the two yoke faces parallel to the horizontal movement of the Hall probe. To correct for the uncertainty of the position of the sensitive part of the Hall probe with respect to its support, we require finally that the field values in the two measurement modes (from here on called "normal" and "reverse") at the magnet centre are the same within the probe reading sensitivity (0.5 G). This final calibration of our ideal reference system is made possible by the gradient in the magnet. The last check is to perform a "transverse" scan, perpendicular to the nominal trajectory of the particle inside the magnet (namely an arc of 45° with a nominal length of 0.864 m) at the magnet centre in the two modes.

The field values measured over a 10 cm range coincide within the probe reading sensitivity. The result of such a scan, which corresponds to Figure 5 in the first set of measurements, is shown in Figure 7.

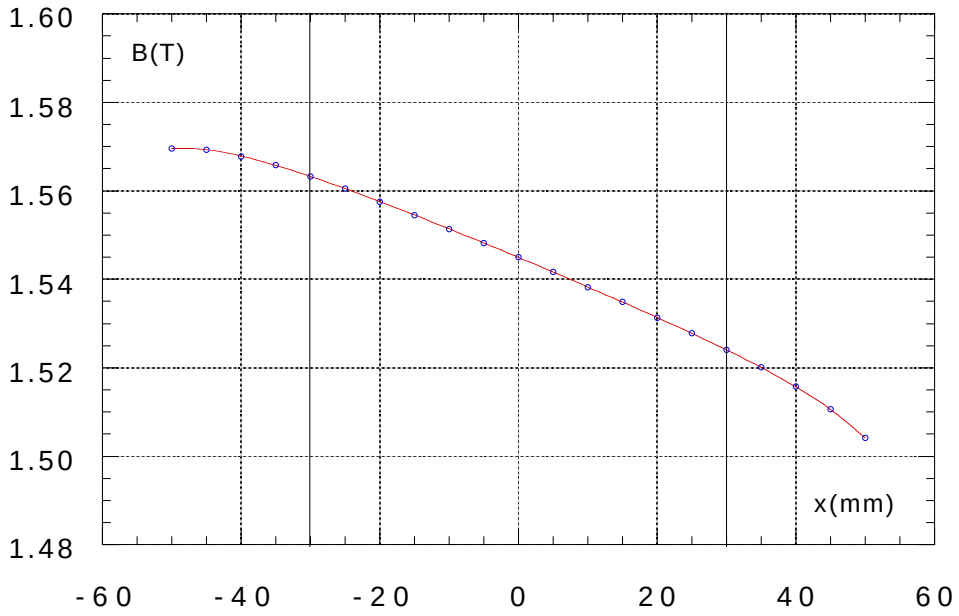

Figure 7 - Horizontal scan at magnet centre.

Taking the derivative of the curve in Figure 7 at the magnet centre, as explained in the preceding section, we find a gradient of 0.655 T/m. The corresponding value of the field index is 0.47, to be compared to the desired value of 0.5. This slight difference can be easily compensated by changing the gradients in the lattice quadrupoles [4,5] by a very small amount. The field quality is shown in Figure 8 (dots), where the field evaluated with POISSON is also given for comparison. It can be observed that there is still a discrepancy between measured and calculated values, but this time the measured field is better than the expected one and almost within the specified tolerance. In addition the main high order contribution is sextupole-like.

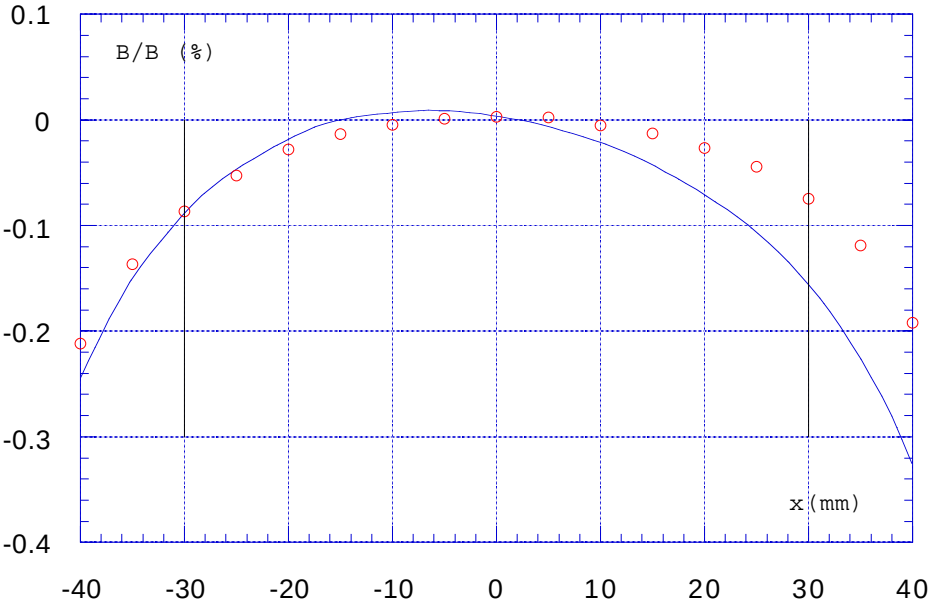

Figure 8 - Field quality at magnet centre.

Figure 9 is the new excitation curve and Figure 10 the vertical field component measured along the nominal trajectory. In this figure, the two vertical lines indicate the boundaries of the nominal trajectory in the rectangular approximation for the field: it can be observed that, due to the short magnet length, there is almost no flat top, so that the usual magnetic length definition (the field integral divided by the field in the flat top region) is not significant in this case.

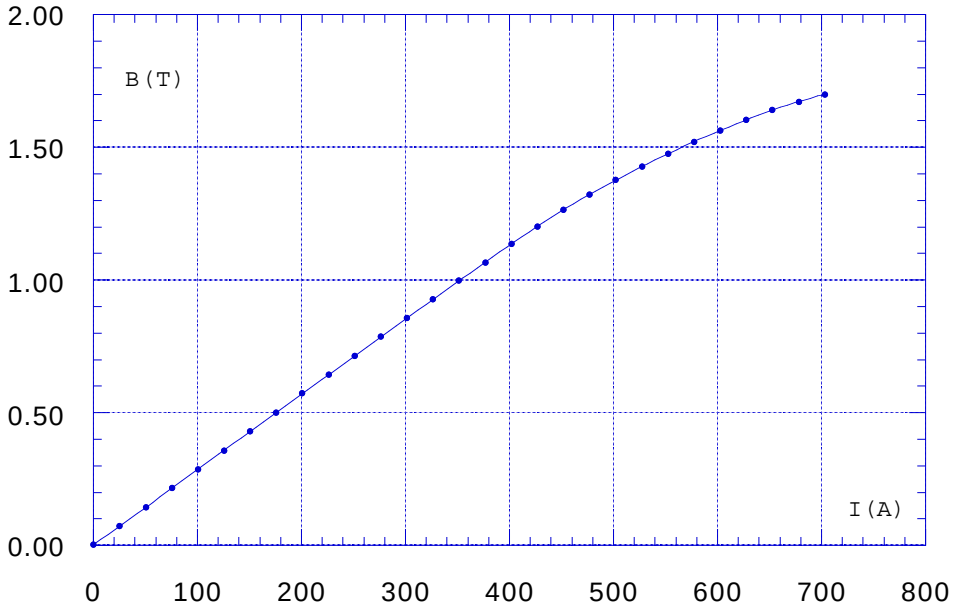

Figure 9 - Excitation curve of the magnet with flat pole profile.

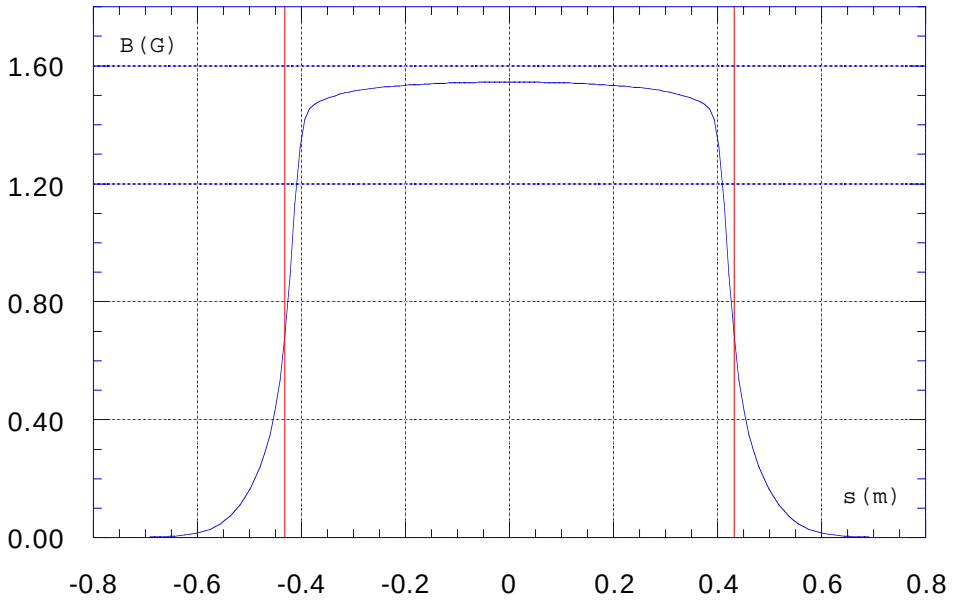

Figure 10 - Vertical field along the nominal trajectory.

In order to estimate the real trajectory of the particles inside the magnet it is necessary to integrate the equation of motion of the particles in the measured field. We have therefore measured the vertical component of the field in steps of 9.6 mm along the ideal trajectory on the horizontal symmetry plane defined as a 45° arc with the ideal length of 0.864 m (the corresponding bending radius is 1.00079 m) and two 35 cm straight segments at its ends. We have also measured the field along trajectories parallel to the ideal one at distances of -3, -2, -1, +1, +2, +3 cm from it. With such a mesh of measured points we can interpolate and get the field at any point in the magnet.

We can set the condition that a particle with the nominal energy is bent by exactly 45° in the dipole by multiplying the measured field by a proper factor. Provided the field is symmetric with respect to the magnet centre, particles travelling on the ideal trajectory before the magnet will follow it also after the magnet. However, there may be two unwanted effects. The first is that the trajectory inside the dipole, due to the fringing field, does not coincide with the ideal one, the second is that the length of the particle trajectory is not the nominal one.

The lowest curve (cut = 0) in Figure 11 shows the displacement of the calculated trajectory of the particles from the ideal one with the field measured on the dipole prototype. It can be seen that the trajectory at the magnet centre is ≈2.3 mm away from its ideal position. Its length is 1.5 mm shorter than the nominal one. Moreover, the field is sufficiently symmetric with respect to the magnet center, so that there is no appreciable displacement of the orbit from the ideal one at the magnet end.

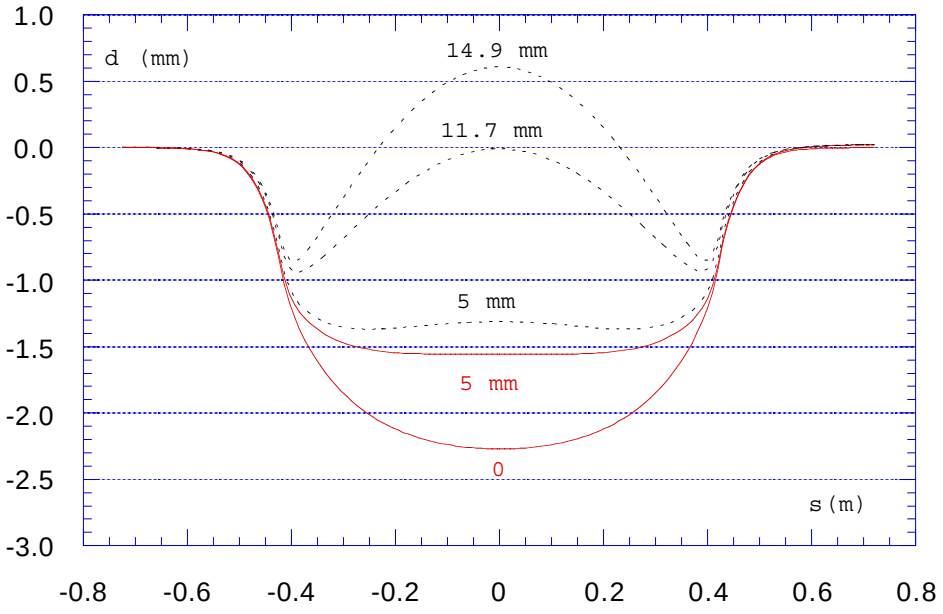

Figure 11 - Distance between calculated and nominal trajectory in the dipole.
Full lines correspond to measured fields, dotted to calculated ones.
The labels near the curves indicate the depth of the cut performed on each end cap.

The shape of the trajectory depends on the field distribution, which in turn depends on the steel length. We have therefore simulated the dependence of the trajectory on the steel length by simulating a cut on the end caps, simply shifting all field values by given displacements. The dotted curve in Figure 11 labeled "5 mm" shows the simulated trajectory obtained by cutting the end caps by 5 mm each; with the end caps shortened by 11.7 mm the distance of the trajectory at the magnet centre from the ideal one vanishes. Cutting the end poles by 14.9 mm makes the length of the trajectory equal to the nominal one. All curves obtained by simulated fields are shown as dotted lines, while those coming from measured field values are full lines. Of course this kind of simulation does not take into account saturation effects on the end caps, and can therefore differ to some extent from the real result.

The difference in total ring circumference can be easily compensated by changing the RF frequency ($\Delta f \approx 30$ KHz out of 74 MHz). However there is a problem of synchronisation in injecting from the Accumulator into the Main Rings, implying the Accumulator length being exactly one third of the Main Ring one. Unfortunately we still do not have the prototypes of Main Ring dipoles, and cannot therefore adjust the magnetic length of the Accumulator dipoles to the right value, which would be the best thing to do, provided the optics of the Main Rings is much more sensitive to this parameter than the Accumulator one. We can at present only rely on magnetic calculations, which foresee a stronger shortening of the trajectory in the Main Rings dipoles, particularly in those magnets with parallel end faces. We have therefore decided on this basis to make a parallel cut of 5 mm on the removable end caps of the prototype, thus keeping the angle between the pole ends always at 45°.

The full line curve labeled "5 mm" in Figure 11 shows the trajectory calculated from the measured field after cutting the end caps by 5 mm, to be compared with the simulated one (dotted line). The length of the trajectory in the dipole is 1.1 mm shorter than the nominal one.

In order to estimate the nonlinear contributions to the dipole magnetic field, we can use the same field maps described before. The mesh points are chosen in such a way that we have 7 transverse points for each azimuthal position along the nominal trajectory. We can therefore find the best polynomial fit to these points and plot the coefficients as a function of the azimuthal position. We have restricted the expansion to the decapole term. We define the field as a function of the transverse position as:

$$B(x) = b_0 + b_1 x + b_2 x^2 + b_3 x^3 + b_4 x^4$$

Figures 12, 13 and 14 show the behaviour of b_1, b_2 and b_4. b_0 does not differ significantly from the behaviour in Figure 10 and the contribution of the octupole term b_3 is negligible.

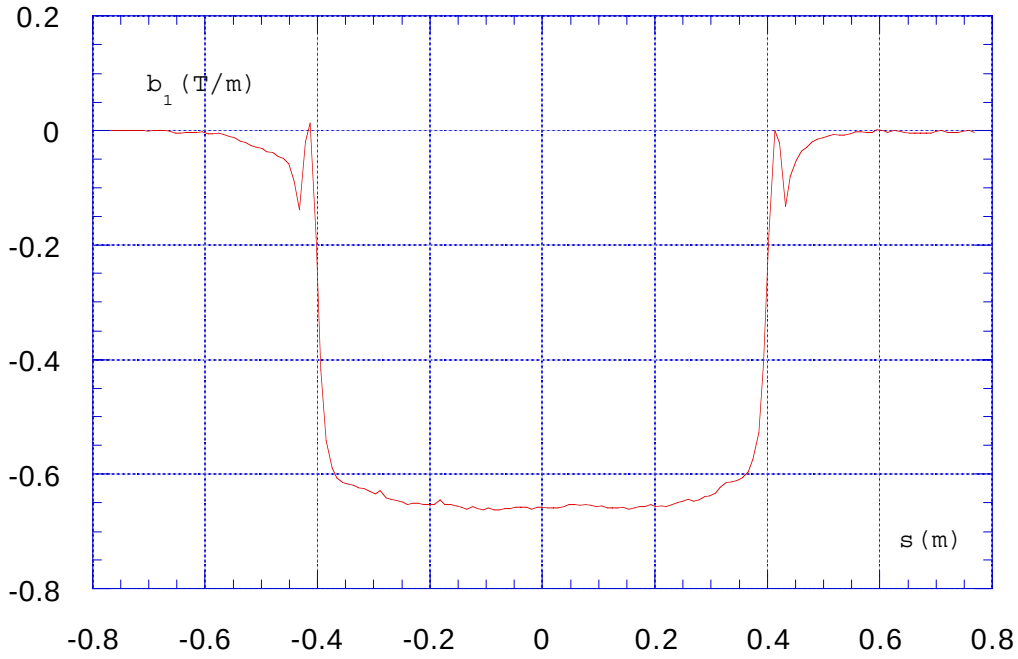

Figure 12 - First order component of transverse expansion.

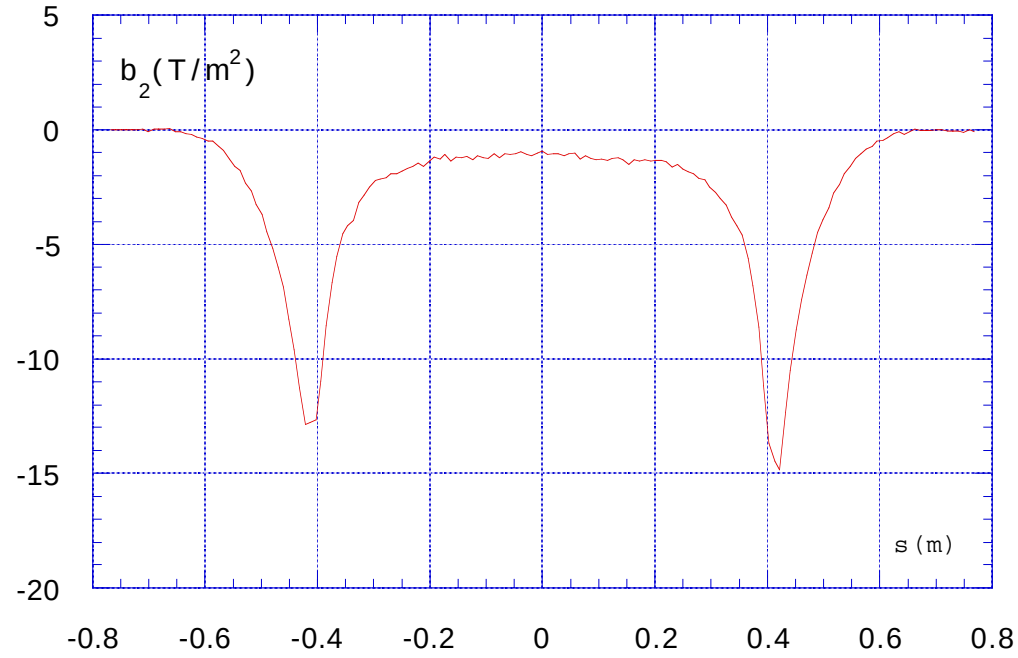

Figure 13 - Second order term of transverse expansion.

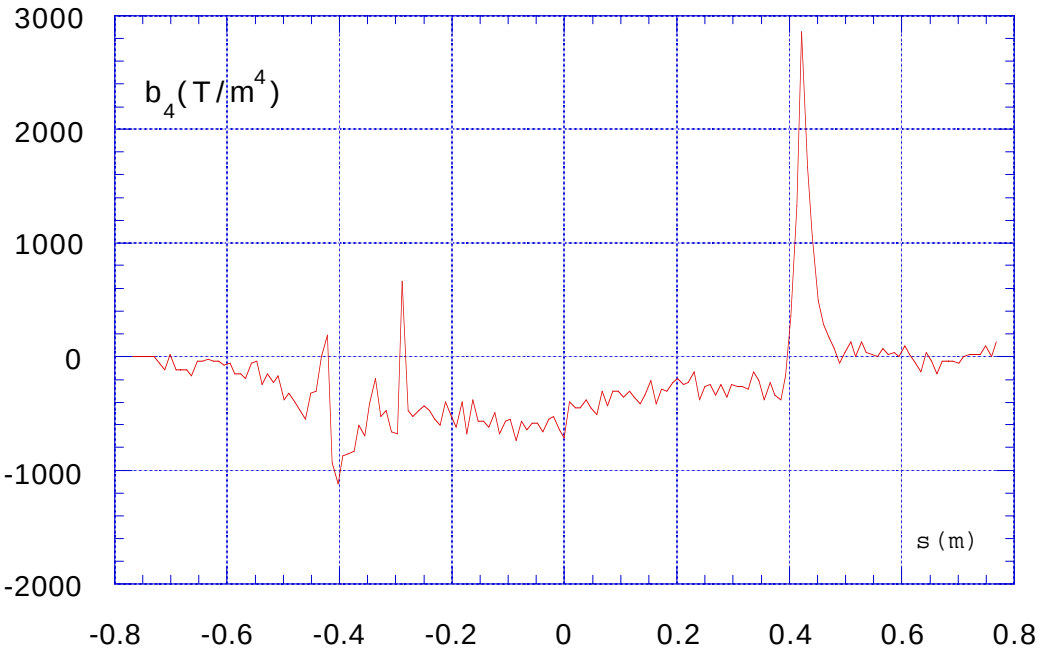

Figure 14 - Fourth order term of transverse expansion.

From the observation of these figures two considerations can be made. The first is that the asymmetry with respect to the magnet centre, negligible from the point of view of the trajectory, shows up clearly in the high order multipolar terms. This asymmetry comes from the electric and hydraulic connections to the coils, which are on one side of the magnet only.

The second important observation (see Figure 13) is that the integrated sextupole term is much larger than simply the second order coefficient at the magnet centre multiplied by the magnet length, the main contribution coming from the fringing field region. We have calculated the contribution to the chromaticity of the ring coming from the second order term of the field expansion in the magnet, and found it almost as large as the "natural" one, namely that coming from the "ideal" machine without high order terms in the magnetic fields. Although this effect can be corrected by means of the lumped sextupoles in the lattice, the required gradients almost exceed the maximum values allowed by the sextupole design [6].

We decided therefore, following the experience of the SLAC damping ring and the Brookhaven compact synchrotron radiation source, to apply a pair of shims on each removable end cap, as shown in Figure 15, where the final configuration is given. The shims exactly cover the end cap outer surface up to a distance of 45 mm from the pole centre. We have tried several different shim geometries. Here we describe the results of the most significant ones:

no shim = end caps without shims after the above described shortening by 5 mm

shim 1 = shim configuration shown in Figure 15

shim 2 = same as shim 1, but with double shim thickness (18 mm).

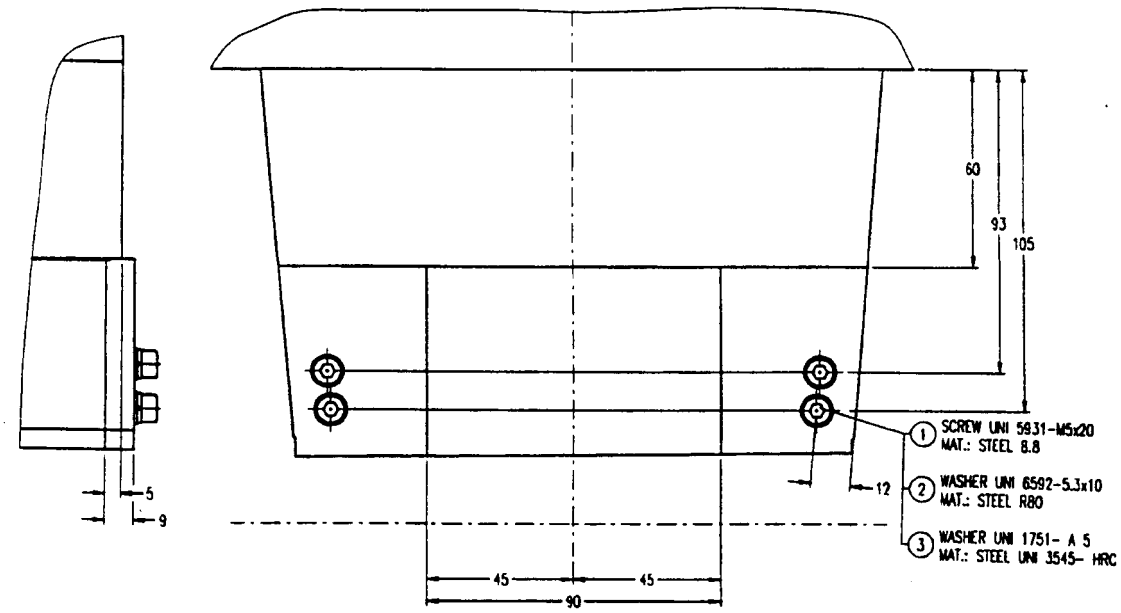

Figure 15 - Final configuration of removable end cap with 5 mm cut and shim 1.

The measurement have been performed only on the "normal" side of the dipole. It should be kept in mind that the measurement have been made with a shim shape slightly different from that shown in Figure 15: some iron was necessarily taken away from the inner side of the shim to leave space for removing the locating pins of the removable end caps. Figure 16 shows the behaviour of the sextupole term for the three shim configurations on the "normal" side of the magnet.

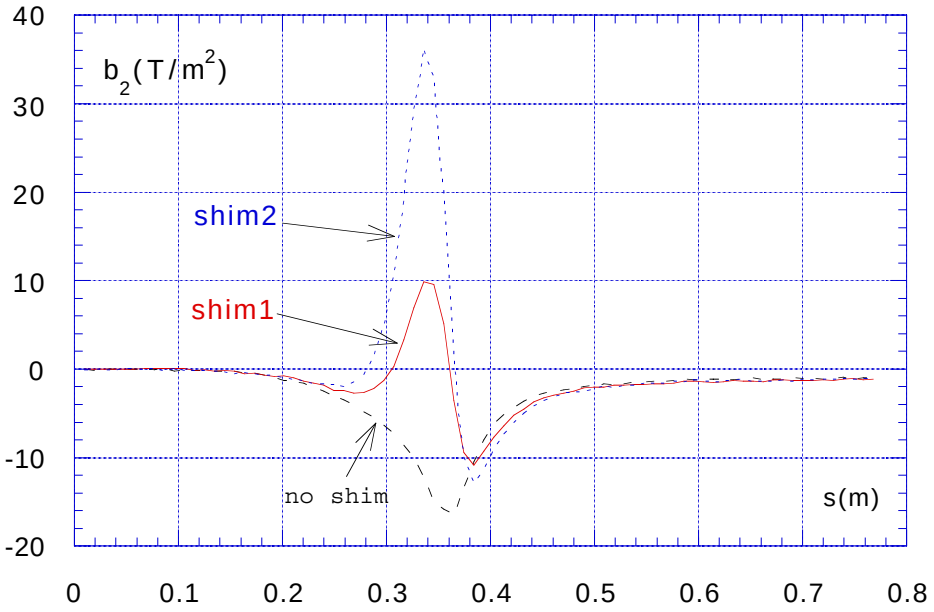

Figure 16 - Second order term with shimmed end cap (dashes = no shim, solid = shim 1, dots = shim 2).

It can be noticed that shim 2 makes the integrated sextupole term almost vanish, while shim 1 reduces the unshimmed value by a factor ≈2. Table V gives the integrated sextupole term in a single bending magnet (obtained from the measurement on the "normal" side multiplied by 2) and the total machine chromaticity (with sextupoles off) including the dipole sextupole term for the three shim configurations.

TABLE V - Chromaticity of the ring with sextupole contribution from the dipoles

	Natural	No shim	Shim 1	Shim 2
$\int b_2\, ds$ (T/m)		-4.3	-2.0	+0.4
Horizontal chromaticity	-4.4	-7.7	-5.3	-3.9
Vertical chromaticity	-4.2	-0.4	-2.3	-4.3

It is clear that shim 2 almost corrects the unwanted contribution of the dipole sextupole term to the total chromaticity. However, the shims have an effect also on the higher order terms, as shown in Figure 17 (octupole), and Figure 18 (decapole). The octupole term, although larger than the unshimmed case, is still very small, while the decapole tends to reach high values.

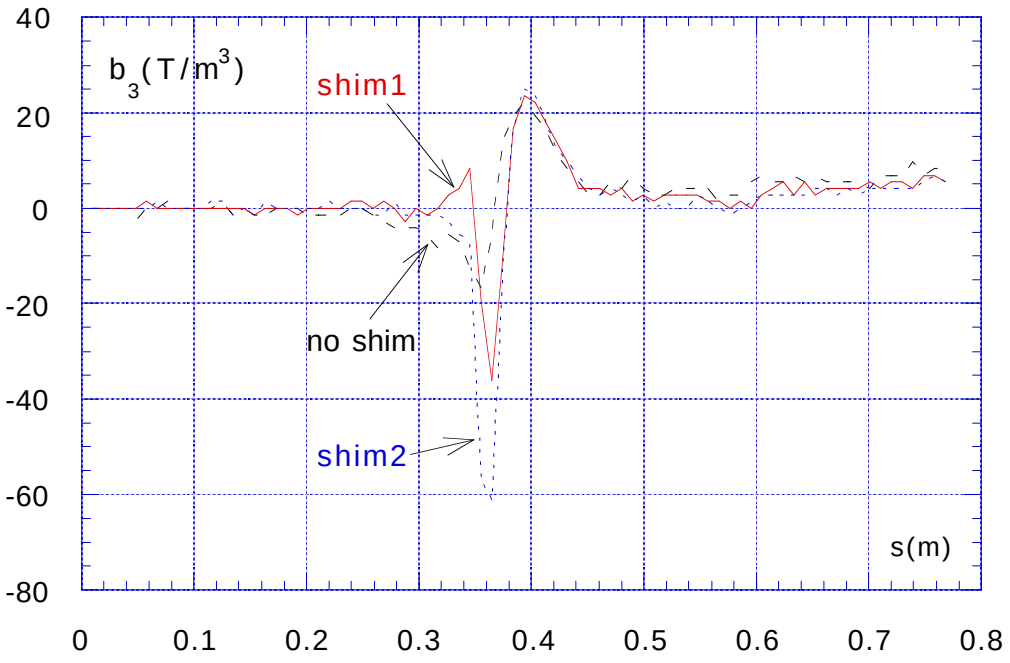

Figure 17 - Third order term with shimmed end cap (dashes = no shim, solid = shim 1, dots = shim 2).

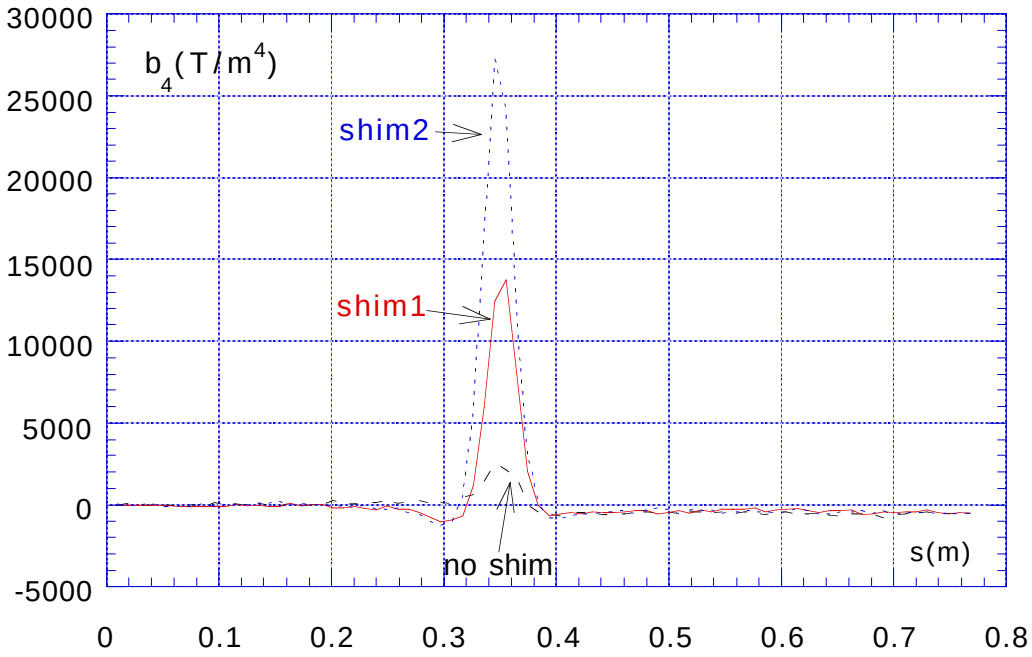

Figure 18 - Fourth order term with shimmed end cap
(dashes = no shim, solid = shim 1, dots = shim 2).

In order to choose the best shim thickness, we have simulated the non-linear behavior of the beam by estimating the dynamic aperture with the program PATRICIA. Non linear terms up to the fourth order have been inserted into the lattice as thin lenses in 11 points per magnet with an intensity proportional to the corresponding integrated multipole for each dipole slice.

The result for the initial configuration without shims is shown in Figure 19.

The large curve, including all the other ones, is the "ideal" dynamic aperture, calculated without high order terms in the magnetic field, with the lumped sextupoles in the lattice set to correct both chromaticities to zero. The dashed curve represents the dynamic aperture which takes into account the sextupole term in the dipoles, again correcting the total chromaticity to zero by means of the lumped sextupoles. The solid line takes into account, in addition, also the measured octupole and decapole terms. For comparison, the dot/dashed rectangle inside all other curves shows the physical aperture of the ring. It is clear in this case that the contribution of terms higher than the second does not change the situation much, while there is a strong reduction of the dynamic aperture coming directly from the necessity of increasing the strength of the lumped sextupoles to correct the large horizontal chromaticity of the ring.

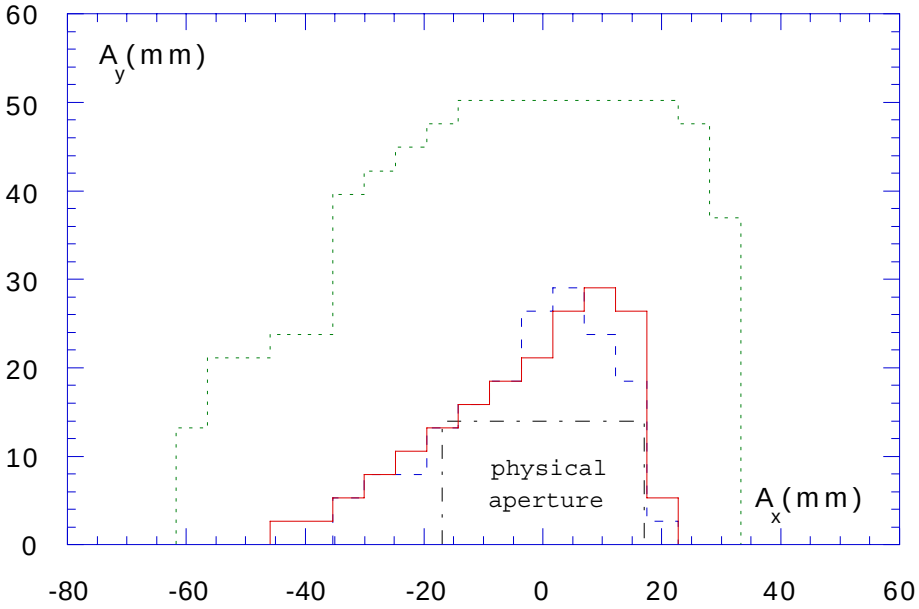

Figure 19 - Dynamic apertures without shims.
(External dots = ideal aperture, dashes = only sextupole term in the dipoles,
solid = sextupoles and multipoles in the dipoles, dot/dashes = physical aperture)

Figure 20 shows the same apertures calculated for the shim 2 configuration. Now the ideal aperture and that calculated with the sextupole term only are almost the same, being the total chromaticity almost unchanged by the higher order terms in the dipole. However, in this case the large fourth order term reduces the dynamic aperture strongly.

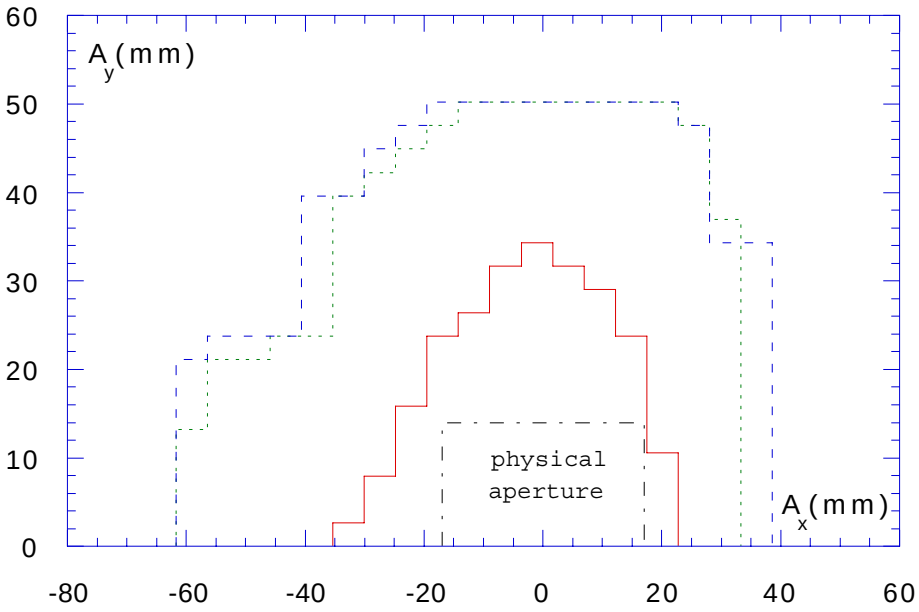

Figure 20 - Dynamic apertures with shim 2.
(External dots = ideal aperture, dashes = only sextupole term in the dipoles,
solid = sextupoles and multipoles in the dipoles, dot/dashes = physical aperture)

Figure 21 shows finally the dynamic aperture in the shim 1 configuration. It is a good compromise between the other two situations, and the region of stable oscillations is well outside the physical aperture. This configuration has therefore been chosen for the series production of the magnets.

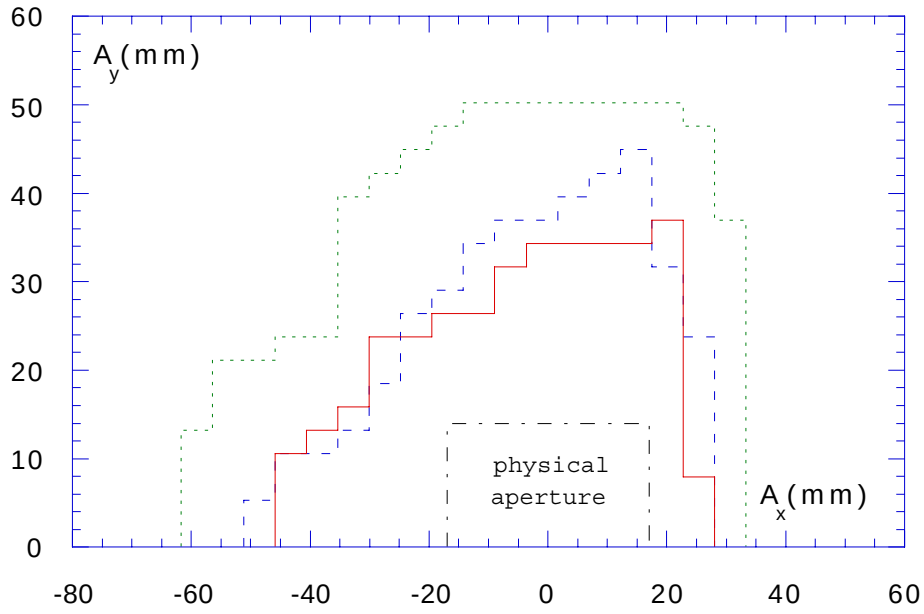

Figure 21 - Dynamic apertures with shim 1.
(External dots = ideal aperture, dashes = only sextupole term in the dipoles, solid = sextupoles and multipoles in the dipoles, dot/dashes = physical aperture)

6. Measurements on the series production

After acceptance of the dipole prototype, the other 7 magnets have been built at TESLA with the same geometry of the modified prototype, namely by shortening the iron length by 5 mm on each side and by adding the end cap shims with the shape shown in Figure 15. The end caps of these 7 magnets are not removable, while the shims are fixed on the poles by means of bolts. In order to make the prototype as similar as possible to the other magnets, the locating pins of the removable end caps have been modified in such a way that the same shim profile is used for all the 8 magnets. The only difference between the prototype and the other dipoles is the presence of the stainless steel locating pins in the prototype, while the poles of the other magnets are full iron.

All the dipoles, including the prototype, have been characterized by measuring the excitation curve, the field at the magnet centre in both the "normal" and "reverse" positions, and a full map, as described in Section 5, on the horizontal symmetry plane within the good field region, at the nominal working point. The maps have been taken at a fixed value of the excitation current, measured by a very precise DCCT device: throughout all the measurements the current has been kept constant (590.625A) within 3×10^{-5}.

The field at the magnet centre has been measured on a straight line perpendicular to the nominal trajectory, as described in Section 4, in steps of 5 mm on a range of ±50 mm, in both the "normal" and "reverse" positions, as a check on the overall alignment procedure. The difference between the two measurement never exceeded 1.5 G.

All the maps on the horizontal plane have been analyzed, as described in Section 5, to get the field integral on the nominal trajectory and the coefficients of the polynomial fit to the transverse variation. These coefficients have been then integrated along the trajectory. The average of these integrals among the 8 magnets yields a good estimate of the magnet field quality, while the spread gives an idea about the construction tolerances.

Figure 22 shows the integrated field on the nominal trajectory as a function of the magnet serial number. The fractional r.m.s. spread is $\pm 7 \times 10^{-4}$, while the accuracy, based mainly on a random alignment error of ±0.2 mm calculated from the uncertainty in the comparison of the "normal" and "reverse" transverse scans at the magnet centre, is $\approx 1 \times 10^{-4}$. Other errors, related to the rotating support system, should be the same for all magnets, and do not affect the value of the spread. We have verified by means of a simulation on the Accumulator lattice, that the effect of this spread on the closed orbit can be easily corrected by means of the orbit correction system.

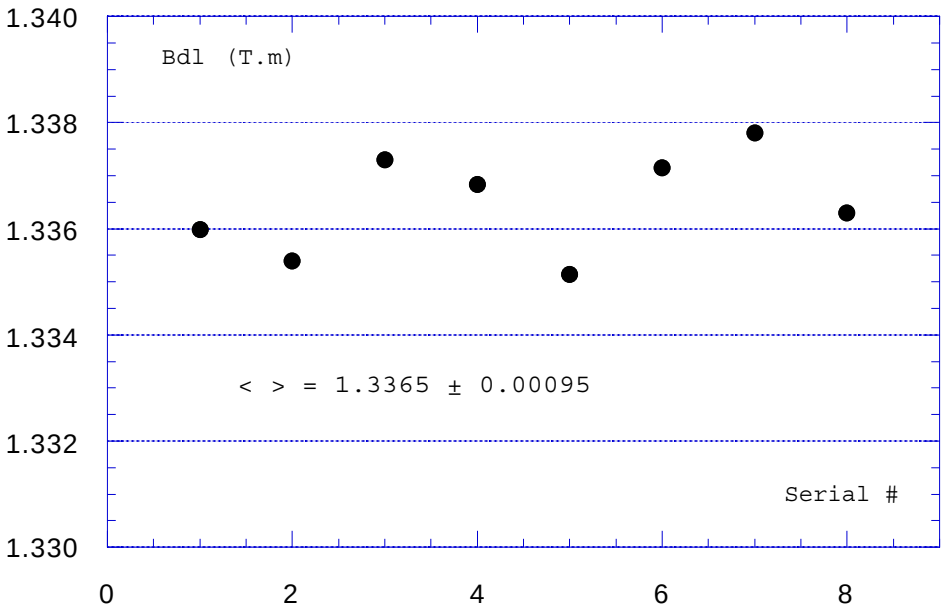

Figure 22 - Integrated field on the nominal trajectory of the 8 dipoles.

Figures 23 through 26 show the distributions of the integrated linear and higher order terms of the transverse expansion, up to the decapole. The octupole component is given for sake of completeness, its contribution within the good field region being one order of magnitude smaller than the decapole. The major contribution to the integrated sextupole and decapole terms come from the fringing field region, as shown in Figures 16 and 18.

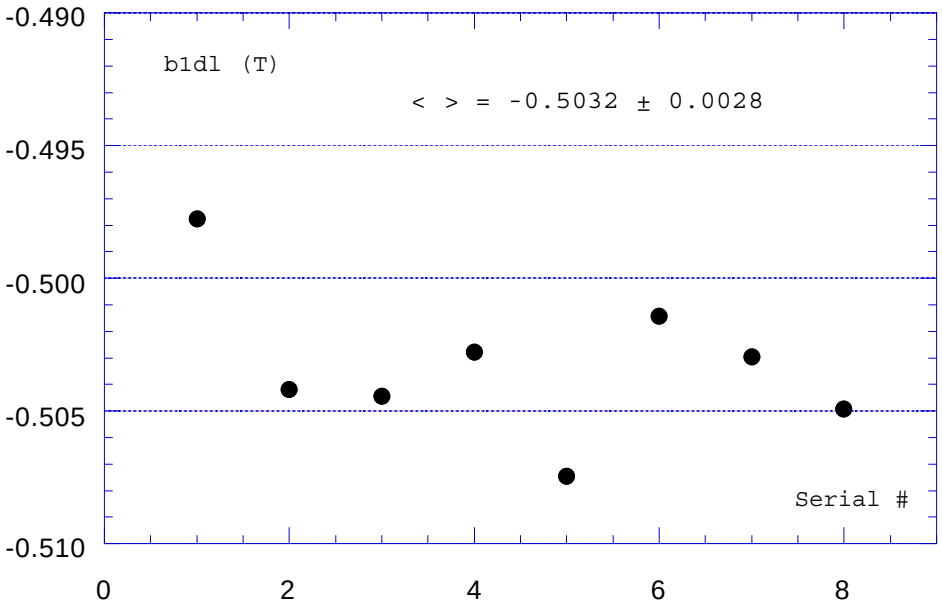

Figure 23 - Integrated gradient of the 8 dipoles.

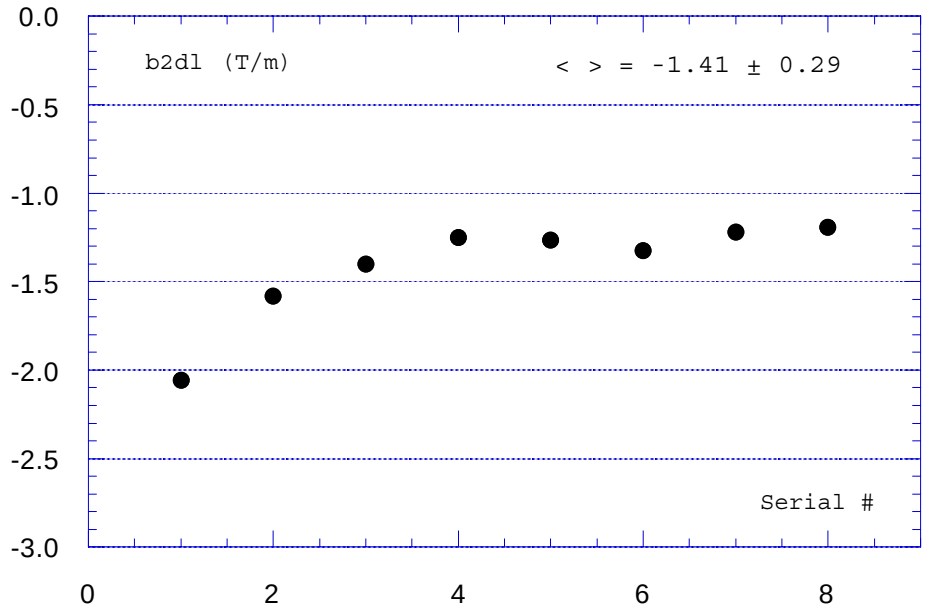

Figure 24 - Integrated second order term of transverse expansion.

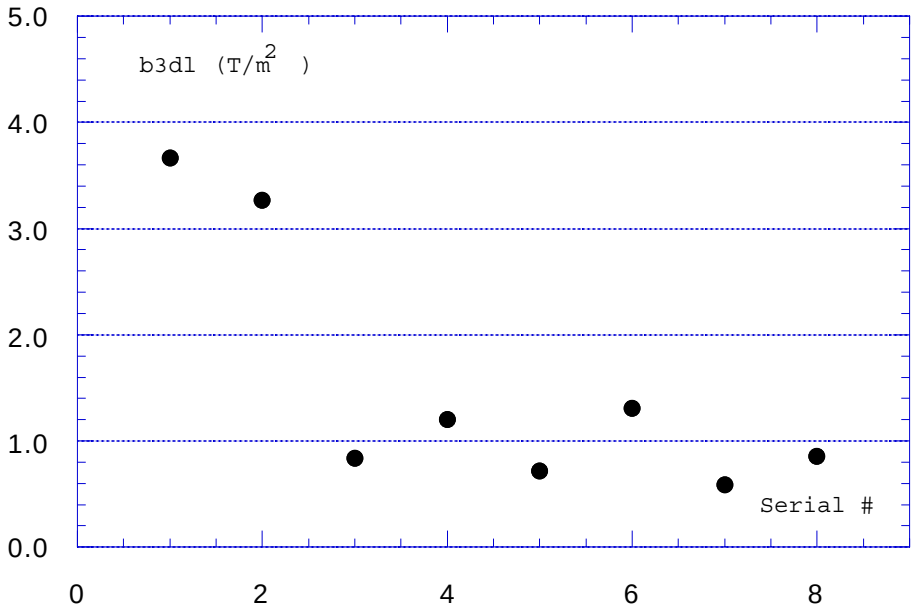

Figure 25 - Integrated third order term of transverse expansion.

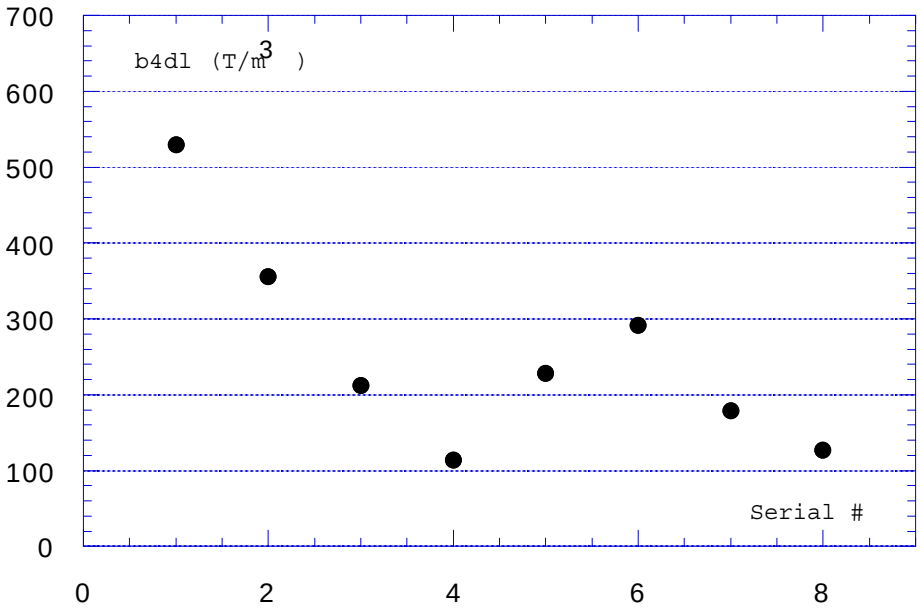

Figure 26 - Integrated fourth order term of transverse expansion.

REFERENCES

[1] M.R. Masullo, C. Milardi, M. Preger "DAΦNE Accumulator update - 3" DAΦNE Technical Note I-9 (13/5/1992).

[2] TESLA Engineering Limited, Storrington, Sussex, RH203EA, England.

[3] OXFORD Instruments, Accelerator Technology Group, Osney Mead, Oxford OX2 0DX, England.

[4] B. Bolli, F. Iungo, M. Modena, M. Preger, C. Sanelli, F. Sgamma, M. Troiani, S. Vescovi "Measurements on TESLA quadrupole prototype for DAΦNE Accumulator and main rings" DAΦNE Technical Note MM-4 (2/12/1994).

[5] B. Bolli, F. Iungo, F. Losciale, M. Paris, M. Preger, C. Sanelli, F. Sardone, F. Sgamma, M. Troiani "Field quality and alignment of the DAΦNE Accumulator quadrupoles" DAΦNE Technical Note MM-8 (21/8/1995).

[6] B. Bolli, F. Iungo, M. Modena, M. Paris, M. Preger, C. Sanelli, F. Sardone, F. Sgamma, M. Troiani "The DAΦNE Accumulator sextupoles" DAΦNE Technical Note MM-6 (10/5/1995).